Effective interactions and shell model studies of heavy tin isotopes

M. P. Kartamyshev, T. Engeland, M. Hjorth-Jensen, and E. Osnes
Department of Physics and Centre of Mathematics for Applications, University of Oslo, N-0316 Oslo, Norway
(Received 5 October 2006; revised manuscript received 26 June 2007; published 17 August 2007)

We present results from large-scale shell model calculations of even and odd tin isotopes from ^{134}Sn to ^{142}Sn with a shell model space defined by the $1f_{7/2}, 2p_{3/2}, 0h_{9/2}, 2p_{1/2}, 1f_{5/2}$, and $0i_{13/2}$ single-particle orbits. An effective two-body interaction based on modern nucleon-nucleon interactions is employed. The shell model results are in turn analyzed for their pairing content using a generalized seniority approach. Our results indicate that a pairing model picture captures a great deal of the structure and the correlations of the lowest lying states for even and odd isotopes.

DOI: 10.1103/PhysRevC.76.024313 PACS number(s): 21.60.Cs, 24.10.Cn, 27.60.+j

I. INTRODUCTION

The region of neutron-rich nuclei around ^{132}Sn with the number of protons at or just below the $Z = 50$ shell closure is an area of current experimental and theoretical interest (see, for example, Refs. [1–10]). Recent results span from β and γ spectroscopy at the CERN on-line isotope mass separator facility (ISOLDE) of the $N = 82$ r-process "waiting point" nucleus ^{130}Cd [4], with several interesting astrophysical implications, to the measurement of the transition strengths $B(E2; 0^+ \rightarrow 2^+)$ and nuclear moments of Te and Sn isotopes at the Holifield Radioactive Ion Beam Facility (HRIBF) at Oak Ridge National Laboratory [2,3,7]. For the latter experiments, the theoretical analysis of Ref. [6], using a quasiparticle random phase approximation, pointed to a weakened pairing strength for the interacting neutrons to explain the experimental results.

A series of experiments at ISOLDE [11] has aimed at decay studies of $^{135-140}$Sn via laser ionization techniques to obtain half-lives and γ-ray spectra for these very neutron-rich Sn nuclides that lie directly in the path of the r process. In Ref. [8] data were presented for $T_{1/2}$ and neutron emission probabilities for $^{135-137}$Sn. Recently, data from various β decays of ^{134,135}Sn were used to confirm and establish new levels in ^{134}Sb and ^{135}Sb [9,10]. Data for β-delayed neutron decays of $A = 137$ and $A = 138$ have also been obtained. These and other data are of importance for our understanding of the presence of a single site for the r-process nucleosynthesis, or at least a single mechanism for elements above $Z = 56$ and possibly a second site/mechanism for elements below $Z = 56$ (see, for example, the discussion in Ref. [4]).

The lifetime of the isotopes $^{136-138}$Sn are of the order of a few milliseconds [8,11], a fact that poses severe limitations on our capability of obtaining spectroscopic information with present laser ionization techniques. Thus, except for the above-mentioned ^{134}Sn isotope and the low-energy spectrum of ^{133}Sn [12], data for heavy tin isotopes ($A = 134$–142) are either rather limited or just missing. Theoretical analyses, except those reported in Refs. [8–10] and a study of two and three valence particles by Coraggio *et al.* [13], provide little spectroscopic information for nuclei beyond ^{135}Sn. The sole exception we are aware of are the mean field investigations of Hofmann and Lenske [14] and Dobaczewski *et al.* [15]. A theoretical analysis of the spectra of these nuclei can therefore provide several possible guidelines for interpretations of data of relevance for astrophysical studies of the r-process path and in particular for the investigation of spectroscopic trends when one moves toward the neutron drip line.

It is within the latter topic that we focus our attention here. The rationale for the present study, in addition to providing spectroscopic information on even and odd Sn isotopes for $A = 134$–142, is to analyze the pairing structure of the low-lying states of these nuclei as we move toward the drip line (the reader should note that the drip line for the Sn isotopes is predicted at $A \sim 160$ [15]). The structure of pairing correlations and the strength of the pairing interaction as one moves toward the drip line, in addition to our understanding of how shells evolve, is a topic of great experimental and theoretical interest in low-energy nuclear physics.

To provide the above-mentioned information on pairing correlations, we perform large-scale shell model calculations using realistic effective interactions. We present results from extensive shell model studies of heavy Sn isotopes with up to ten valence neutrons beyond the ^{132}Sn core. The effective neutron-neutron interaction is tailored for a shell model space that includes the single-particle states $1f_{7/2}, 2p_{3/2}, 0h_{9/2}, 2p_{1/2}, 1f_{5/2}$, and $0i_{13/2}$. A perturbative many-body scheme is employed to derive the effective interaction starting with a realistic model for the free nucleon-nucleon interaction, as detailed in Ref. [16] and reviewed briefly in the next section. The resulting wave functions of selected low-lying states of odd and even Sn isotopes are in turn analyzed for their pairing content using the generalized seniority approach developed by Talmi [17]. This provides one possible way of extracting pairing correlations and information about the pairing strength as one increases the number of valence nucleons.

This article is presented in four sections. In Sec. II we give a brief outline of the theoretical framework for obtaining an effective interaction for the nuclei of interest. Some basic shell model features are also presented. The results from shell model calculations for both even and odd isotopes are presented in Sec. III together with a generalized seniority analysis. Concluding remarks are found in Sec. IV.

II. SHELL MODEL HAMILTONIAN

We give here a brief review of our calculational recipe; for further details, see Ref. [16]. Our scheme to obtain an effective two-body interaction appropriate for heavy tin isotopes starts with a free nucleon-nucleon interaction V appropriate for nuclear physics at low and intermediate energies. Here we employ the potential model of Ref. [18], the so-called charge-dependent Bonn interaction. This is an extension of the one-boson-exchange models of the Bonn group [19], where mesons like π, ρ, η, δ, and ω and the fictitious σ meson are included. Thereafter we need to handle the fact that the strong repulsive core of the nucleon-nucleon potential V is unsuitable for perturbative approaches. This problem is overcome by introducing the reaction matrix G given by the solution of the Bethe-Goldstone equation

$$G = V + V\frac{Q}{\omega - H_0}G, \tag{1}$$

where ω is the unperturbed energy of the interacting nucleons and H_0 is the unperturbed Hamiltonian. The operator Q, commonly referred to as the Pauli operator, is a projection operator that prevents the interacting nucleons from scattering into states occupied by other nucleons. In this work we solve the Bethe-Goldstone equation for five starting energies ω, by way of the so-called double-partitioning scheme discussed in, for example, Ref. [16]. The G matrix is the sum over all ladder type diagrams. This sum is meant to renormalize the strong repulsive short-range part of the interaction. The physical interpretation is that the particles must interact with each other an infinite number of times to produce a finite interaction.

Because the G matrix represents just the summation to all orders of ladder diagrams with particle-particle diagrams, there are obviously other terms that need to be included in an effective interaction. Long-range effects represented by core-polarization terms are also needed. The first step then is to define the so-called $\hat{Q}$ box given by

$$P\hat{Q}P = PGP + P\left(G\frac{Q}{\omega - H_0}G + G\frac{Q}{\omega - H_0}G\frac{Q}{\omega - H_0}G + \cdots\right)P. \tag{2}$$

The $\hat{Q}$ box is made up of nonfolded diagrams that are irreducible and valence linked. We can then obtain an effective two-body interaction, $H_{\rm eff} = \tilde{H}_0 + V_{\rm eff}$, in terms of the $\hat{Q}$ box, with [16]

$$V_{\rm eff}(n) = \hat{Q} + \sum_{m=1}^{\infty}\frac{1}{m!}\frac{d^m\hat{Q}}{d\omega^m}\{V_{\rm eff}(n-1)\}^m, \tag{3}$$

where (n) and $(n-1)$ refer to the effective interaction after n and $n-1$ iterations. The zeroth iteration is represented by just the $\hat{Q}$ box. Observe also that the effective interaction $V_{\rm eff}(n)$ is evaluated at a given model space energy ω, as is the case for the G matrix as well. Here we choose $\omega = -20$ MeV. Less than ten iterations were needed to obtain a numerically stable result. All nonfolded diagrams through the third order in the interaction G are included. A harmonic oscillator basis was used to derive the single-particle radial wave functions with an oscillator energy $\hbar\omega = 7.87$ MeV. For further details, see Ref. [16].

The present neutron-neutron interaction, the corresponding proton-proton interactions, and the proton-neutron interactions derived for holes and particles states using ^{132}Sn as closed shell core have been employed in several shell model calculations of nuclei around ^{132}Sn (see, for example, Refs. [4,9,10,20–22]).

The effective two-particle interaction can in turn be used in shell model calculations. The shell model problem requires the solution of a real symmetric $n \times n$ matrix eigenvalue equation,

$$\tilde{H}|\Psi_k\rangle = E_k|\Psi_k\rangle, \tag{4}$$

with $k = 1, \ldots, K$. At present our basic approach to finding solutions to Eq. (4) is the Lanczo's algorithm; an iterative method that gives the solution of the lowest eigenstates. This method was applied to nuclear physics problems by Whitehead *et al.* in 1977. The technique is described in detail in Ref. [23] and implemented via the Oslo shell model code [24]. The eigenstates of Eq. (4) are written as linear combinations of Slater determinants in the m scheme, distributing the N valence neutrons in all possible ways through the single-particle m-scheme orbitals of the model space, $1f_{7/2}, 2p_{3/2}, 0h_{9/2}, 2p_{1/2}, 1f_{5/2}$, and $0i_{13/2}$. As seen in Table I, the dimensionality n of the eigenvalue matrix $\tilde{H}$ increases rapidly with the increasing number of valence particles and, for the Sn isotopes of interest, can take values up to $n \approx 6 \times 10^7$.

The single-particle energies are extracted from the experimental ^{133}Sn spectrum [12], except for the $0i_{13/2}$ single-particle orbital that lies above the ^{132}Sn + n threshold 2.45(5) MeV [25]. If one interprets the 2434-keV level in ^{134}Sb as the $(\pi g_{7/2}, \nu i_{13/2})10^+$ configuration [26], the position of the $0i_{13/2}$ orbital can be estimated to be 2.6940 ± 0.2 MeV. The adopted single-particle energies used in this work are displayed in Fig. 1.

We anticipate parts of the discussion of our results by pointing to the fact that there is a difference of 0.85 MeV between the ground state in ^{133}Sn and the first excited state $(3/2)^-$ and of 1.56 MeV to the next excited state with spin and parity assignment $(9/2)^-$. Furthermore, the shell gap for neutrons is

$$\begin{aligned}\Delta\epsilon_\nu &= \epsilon_\nu(1f_{7/2}) - \epsilon_\nu(0g_{7/2}) \\ &= [\mathrm{BE}(^{132}\mathrm{Sn}) - \mathrm{BE}(^{133}\mathrm{Sn})] + [\mathrm{BE}(^{132}\mathrm{Sn}) - \mathrm{BE}(^{131}\mathrm{Sn})] \\ &= 4.84\ \mathrm{MeV}.\end{aligned} \tag{5}$$

The first excited negative parity state in ^{132}Sn has an excitation energy of 4.351 MeV and total angular momentum $J^\pi = 3^-$.

TABLE I. Total number of basis states for the shell model calculation with the single-particle orbitals $1f_{7/2}, 2p_{3/2}, 0h_{9/2}, 2p_{1/2}, 1f_{5/2}$, and $0i_{13/2}$ defining the model space.

System	Dimension	System	Dimension	System	Dimension
^{134}Sn	62	^{137}Sn	34 804	^{140}Sn	4 606 839
^{135}Sn	448	^{138}Sn	207 514	^{141}Sn	17 574 855
^{136}Sn	4 985	^{139}Sn	1 049 533	^{142}Sn	59 309 576

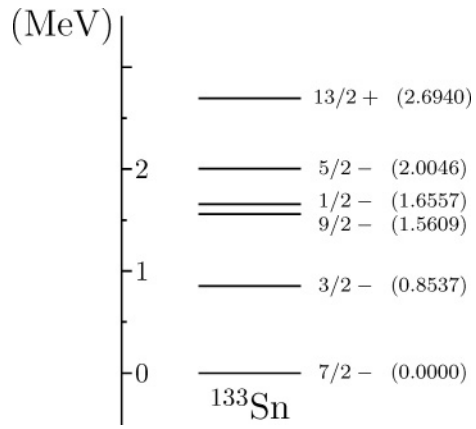

FIG. 1. Adopted single-particle energies for the orbitals $1f_{7/2}$, $2p_{3/2}$, $0h_{9/2}$, $2p_{1/2}$, $1f_{5/2}$, and $0i_{13/2}$ in shell model calculations.

This indicates that the contribution from the two-body interaction is of the order of ∼0.5 MeV if we assume a particle-hole model space consisting of the above-mentioned single-particle states. Compared with closed-shell cores like ^{16}O, ^{40}Ca, and ^{56}Ni, the cross-shell interaction for the present study is much weaker, almost an order of magnitude compared with a similar analysis for ^{16}O (in ^{16}O the shell gap for neutrons is 11.521 MeV and the first excited negative parity state $J^\pi = 3^-_1$ is located at 6.129 MeV). This fact applies to the matrix elements of the derived two-body interaction as well, an expected feature because the valence neutrons are on average further apart from each other. An investigation of such trends of the effective interactions for nuclei from ^{4}He to ^{208}Pb was done in Ref. [27]. There the authors demonstrated that the interaction matrix elements for valence particle systems become on average smaller with increasing mass number A.

In the analysis of the pairing content of our results, we see that the interplay between the single-particle spacing in ^{133}Sn and the strength of the two-body interaction allows a qualitative understanding of the reported results.

III. RESULTS AND DISCUSSION

In this section we present results of the shell model calculations for Sn isotopes with up to ten valence neutrons beyond the ^{132}Sn closed-shell core. As the experimental data available at the present time for the $A \geqslant 134$ tin isotopes are quite sparse, we have a limited possibility of checking the validity of our effective interaction in this region of the nuclear chart. Hence, most of the present results are of a predictive character, providing shell model guidelines for future experiments of the $A \geqslant 134$ tin isotopes.

Before we proceed with the spectra for odd and even isotopes, we present in Table II the theoretical binding energies, compared with the few available experimental data, together with the corresponding neutron and two-neutron separation energies.

For the light isotopes, and where data are available, there is a fair agreement between theory and experiment, irrespective of the fact that our Hamiltonian does not include three-body interactions. The latter are known to add a particle-dependent correction; see, for example, the recent estimations of Zuker [28]. The binding energies, for both even and odd isotopes, show an increasing trend with increasing mass number, most likely an effect due to the omission of three-body interactions. From the above separation energies, there is no sign of a diminishing value of S_n with increasing A, supporting the estimations from mean field calculations [15]). Mean field calculations predict the drip line for Sn isotopes at $A \sim 160$.

A. Even tin isotopes

The results of the shell model calculation for the even tin isotopes are displayed in Table III for selected positive parity states. We obtain a rather good agreement with the measured energies of the positive parity yrast states in ^{134}Sn [8,29]. In our presentation we have omitted the negative parity states. In our model they are constructed from particle excitations and the first states appear at ∼4–5 MeV. This is also a region where we expect, from the shell gap of Eq. (5), negative parity particle-hole excitations to appear.

Of particular interest here is that the 0^+_1–2^+_1 spacing remains nearly constant, except for a small increase at ^{140}Sn due to the filling of the $1f_{7/2}$ single-particle orbit. This constancy is similar to what we have for the lighter even tin isotopes, from ^{102}Sn to ^{130}Sn. The difference is that the gap is smaller by approximately 0.5 MeV. Compared with the matrix elements for the model space of the lighter tin isotopes (the model space for ^{102}Sn to ^{130}Sn consists of the single-particle orbits $0g_{7/2}$, $2s_{1/2}$, $0h_{11/2}$, $1d_{3/2}$, and $1d_{5/2}$), the interaction matrix elements are on average smaller for the present model space. This is simply due to the fact that the nucleons are farther

TABLE II. Binding energies (BE), neutron separation energies S_n, and two-neutron separation energies S_{2n} for the tin isotopes from ^{134}Sn to ^{142}Sn. The first row for each entry represents the results from our calculations, while the second row represents experimental data, where available.

	^{134}Sn	^{135}Sn	^{136}Sn	^{137}Sn	^{138}Sn	^{139}Sn	^{140}Sn	^{141}Sn	^{142}Sn
BE	−1.312	−1.307	−2.679	−2.606	−4.010	−3.806	−4.888	−5.034	−6.443
	−1.444	−1.094	−2.355	−1.768					
S_n	3.782	2.465	3.842	2.397	3.874	2.265	3.553	2.615	3.879
	3.914	2.075	3.776	1.877					
S_{2n}	6.252	6.247	6.307	6.239	6.271	6.140	5.818	6.168	6.495
	6.384	5.989	5.851	5.654					

TABLE III. Selected low-lying states for ^{134}Sn, ^{136}Sn, ^{138}Sn, ^{140}Sn, and ^{142}Sn. Experimental data for ^{134}Sn were taken from Refs. [8,29]. All entries are in MeV.

	^{134}Sn		^{136}Sn		^{138}Sn		^{140}Sn		^{142}Sn	
J_i^π	Theory	Experiment	J_i^π	Theory	J_i^π	Theory	J_i^π	Theory	J_i^π	Theory
0_1^+	0.0000	0.0000	0_1^+	0.0000	0_1^+	0.0000	0_1^+	0.0000	0_1^+	0.0000
0_2^+	2.2822		0_2^+	1.8779	0_2^+	1.5280	0_2^+	1.2256	0_2^+	1.1925
1_1^+	2.4141		1_1^+	1.9571	1_1^+	2.0327	1_1^+	2.0539	1_1^+	1.6911
2_1^+	0.7748	0.7256	2_1^+	0.7339	2_1^+	0.7615	2_1^+	0.8028	2_1^+	0.7734
2_2^+	1.6601		2_2^+	1.4642	2_2^+	1.2840	2_2^+	1.3293	2_2^+	1.3338
3_1^+	2.0978		3_1^+	1.8183	3_1^+	1.6072	3_1^+	1.5394	3_1^+	1.6741
4_1^+	1.1161	1.0734	4_1^+	1.1614	4_1^+	1.3550	4_1^+	1.4381	4_1^+	1.5690
4_2^+	1.9486		4_2^+	1.3332	4_2^+	1.5171	4_2^+	1.6308	4_2^+	1.6471
5_1^+	2.1708		5_1^+	1.6877	5_1^+	1.8158	5_1^+	1.7667	5_1^+	1.9226
6_1^+	1.2582	1.2474	6_1^+	1.3770	6_1^+	1.5288	6_1^+	1.8969	6_1^+	1.9856
6_2^+	2.6215		6_2^+	2.1620	6_2^+	2.1359	6_2^+	2.0722	6_2^+	2.1338
7_1^+	2.9538		7_1^+	2.2915	7_1^+	2.1221	7_1^+	2.1126	7_1^+	2.2372
8_1^+	2.4634	2.5089	8_1^+	2.1189	8_1^+	2.3606	8_1^+	2.4042	8_1^+	2.5904
8_2^+	4.6571		8_2^+	2.4125	8_2^+	2.7503	8_2^+	2.6369	8_2^+	2.899

apart on average from each other than they are for the lighter tin isotopes. For the 0_1^+–2_1^+ spacing, the most important configurations are those where the single-particle orbits $2p_{3/2}$ and $1f_{7/2}$ are involved while the $0h_{9/2}$ plays a role in excited states with higher spin values, as expected from the single-particle spectrum of Fig. 1. Actually, the gross features of both the even and odd low-energy spectrum can be captured by an interaction defined for a model space including only the $2p_{3/2}$ and $1f_{7/2}$ orbits. This feature is similar to what we have in the calcium isotopes, except that the $1p_{3/2}$ and $0f_{7/2}$ orbits have one node less. These properties of the calcium isotopes were discussed more than 40 years ago (see, for example, Refs. [30,31]).

The matrix elements that involve the $2p_{3/2}$ and $1f_{7/2}$ orbits oscillate in absolute value between ∼0.5 and 1.0 MeV. This means, if we adopt a simple pairing model analysis, as was done in Ref. [32], that the relation between the single-particle spacing and the interaction matrix elements is of the order of ∼0.5–1.0. Within the framework of a simple pairing model, this is a region where we expect pairing correlations to play a dominant role. In this case, the interaction determines much of the pairing gap, viz., the difference between the seniority zero ground state and the first excited seniority two state, where we have one broken pair. As we show in Secs. III C and III D, a generalized seniority analysis indicates indeed that pairing correlations are still strong, resulting in a nearby constant 0_1^+–2_1^+ spacing, as is the case for the lighter Sn isotopes. See also the discussion in Ref. [32].

The results for the $B(E2)$ calculations are shown in Table IV. The values of calculated $B(E2)$ transition probabilities are presented in Weisskopf units (W.u.) as defined in Ref. [33]. Experimental values of $B(E2)$ for the nuclei of interest are currently available only for two transitions in ^{134}Sn: $B(E2: 6_1^+ \to 4_1^+) = 0.88 \pm 0.17$ W.u. [34] and $B(E2: 0_1^+ \to 2_1^+) = 7.24$ W.u. [2]. These transitions probabilities can be reproduced in our calculations by adjusting the effective neutron charge value to $e_n^{\text{eff}} = 0.66\ e$ for the $6_1^+ \to 4_1^+$ transition and $e_n^{\text{eff}} = 0.62\ e$ for the $0_1^+ \to 2_1^+$ transition, respectively.

One could derive state-dependent effective charges along the same lines as those for the effective interaction. In this work, however, we limit ourselves to a constant effective charge. An average of the neutron effective charge obtained above, $e_n^{\text{eff}} = 0.64\ e$, has been used for every calculated transition. It should be noted that the authors of Ref. [8] use a similar value, $e_n^{\text{eff}} = 0.70\ e$

The $B(E2: 2_1^+ \to 0_1^+)$ values scale nicely with the number of valence neutrons, except for ^{142}Sn, where we see a reduction due to the weak shell closure at ^{140}Sn; see the discussion below on odd isotopes as well. We notice also that the $B(E2: 4_1^+ \to 2_1^+)$ value almost vanishes at ^{138}Sn. From the generalized seniority discussion of Sec. III C, we would expect this value to be large because the seniority $\nu = 2$ overlaps with the shell model wave functions are large for the 2_1^+ and 4_1^+ states. Within the framework of a naive seniority picture the corresponding transition between two seniority $\nu = 2$ states is expected to be larger than the value listed in Table IV. There are, however, other contributions as well that cancel out the naive seniority picture. Furthermore, analyzing the

TABLE IV. Selected $B(E2)$ values for ^{134}Sn, ^{136}Sn, ^{138}Sn, ^{140}Sn, and ^{142}Sn. $e_n^{\text{eff}} = 0.64\ e$. All entries are in W.u.

Transition	^{134}Sn	^{136}Sn	^{138}Sn	^{140}Sn	^{142}Sn
$2_1^+ \to 0_1^+$	1.50	2.94	4.19	5.72	1.96
$4_1^+ \to 2_1^+$	1.53	2.04	0.01	1.71	4.32
$6_1^+ \to 4_1^+$	0.83	0.33	0.27	0.54	0.53
$8_1^+ \to 6_1^+$	0.12	1.25	0.03	0.08	0.50

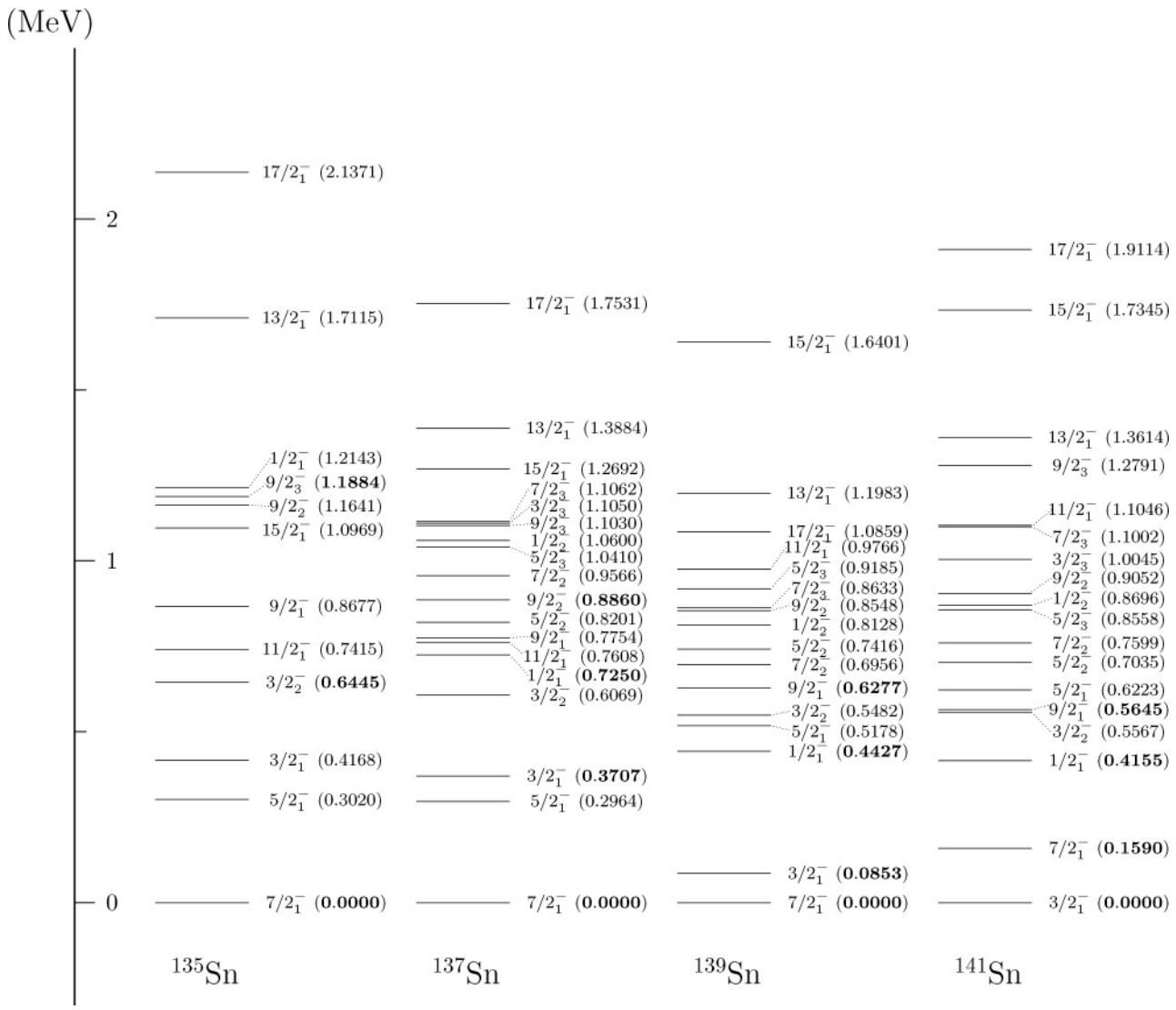

FIG. 2. Selected low-lying states of ^{135}Sn, ^{137}Sn, ^{139}Sn, and ^{141}Sn. All entries are in MeV. Boldfaced numbers represent states with the largest one-quasiparticle content; see discussion in Sec. III E. For energies below 1.5 MeV we list up to three states with the same spin for $J^\pi = 1/2^-, 3/2^-, 5/2^-, 7/2^-, 9/2^-$, because these are also discussed in connection with our generalized seniority analysis in Sec. III E. For higher spins we list only the yrast states.

other $B(E2 : 4_i^+ \to 2_1^+)$ transitions, it is the third 4^+ state that exhibits the largest transition, with $B(E2 : 4_3^+ \to 2_1^+) = 1.91$ W.u. A further analysis and interpretation of the structure of the wave functions is made in connection with our generalized seniority analysis in Sec. III C.

B. Odd isotopes

The results of the shell model calculation for the odd isotopes are displayed in Fig. 2. In our pairing analysis below we show that, except for the ground states and the lowest lying $3/2^-$ states, most of the other states displayed in Fig. 2 deviate from a one-quasiparticle picture. We postpone, therefore, an analysis of the odd isotopes to the generalized seniority analysis below (see Sec. III C). In connection with the generalized seniority analysis, we would, however, like to guide the eye to the evolution of the $(1/2)^-, (3/2)^-, (5/2)^-, (7/2)^-$, and $(9/2)^-$ states as functions of A. These states can be well represented by a one-quasiparticle picture, and the energies of these states plunge down in the spectrum with increasing A, a feature shown in Fig. 2. States with a one-quasiparticle character are shown with bold values for the energies. Other states, such as the first $(1/2)^-$ and $(5/2)^-$, which also plunge down in the spectrum with increasing A, are more fragmented in ^{135}Sn and ^{137}Sn, as discussed in Sec. III E. The $(11/2)^-$ and $(15/2)^-$ states are more complex many-body states.

For the sake of completeness, in Table V we display also selected $B(E2)$ transition probabilities from the first excited state to the ground state. We have used the effective neutron charge value of $e_n^{\text{eff}} = 0.64\ e$. The shell closure in ^{140}Sn is reflected in these transitions as well.

TABLE V. $B(E2)$ for ^{135}Sn, ^{137}Sn, ^{139}Sn, and ^{141}Sn for the lowest states. $e_n^{\rm eff} = 0.64\,e$. All entries are in W.u.

Transition	^{135}Sn	^{137}Sn	^{139}Sn	^{141}Sn
$(3/2)_1^- \rightarrow (7/2)_1^-$	1.66	0.27	0.005	
$(7/2)_1^- \rightarrow (3/2)_1^-$				0.16

C. Generalized seniority

We here interpret the shell model results in terms of the generalized seniority model [17]. As discussed in Sec. III A for the even Sn isotopes, our calculated energy spectra indicate a strong pairing effect. To further explore this situation we analyze here our complicated shell model wave functions by using the generalized seniority approach [17].

The generalized seniority scheme is an extension of the seniority scheme; that is, from involving only one single orbital in j, the model is generalized to involve a group of j orbitals within a major shell. The generalized seniority scheme is a simpler model than the shell model because a rather limited number of configurations with a strictly defined structure are included. These states can also be given a straightforward physical interpretation because they represent only selected correlations. If we, by closer investigation and comparison of the shell model wave function and the seniority states, find that the most important components are accounted for by the generalized seniority scheme, we can benefit from this and reduce the shell model basis. This would be particularly useful when we want to do calculations of systems with a large number of valence particles. For an even system, states with seniority $\nu = 0$ are by definition states where all particles are paired. Seniority $\nu = 2$ states have one pair broken, seniority $\nu = 4$ states have two pairs broken, etc. The admixture of seniority $\nu = 4$ states into seniority $\nu = 0$ and $\nu = 2$ states has been analyzed by, for example, Bohr and Mottelson [35] and Zhang *et al.* [36]. It was found that for some states the admixture from seniority $\nu = 4$ states could be as large as 20%.

Outside the closed shell, in our case ^{132}Sn, we construct a generalized seniority $\nu = 0$ pair,

$$S^+ = \sum_j \frac{1}{\sqrt{2j+1}} C_j \sum_{m \geqslant 0} (-1)^{j-m} a^+_{jm} a^+_{j-m}\,, \tag{6}$$

and identify the coefficients C_j in the two-particle wave function $S^+|0\rangle$ with the calculated ground state amplitudes of the complete shell model state ^{134}Sn. Similarily, the generalized seniority $\nu = 2$ operators take the form

$$D^+_{\mu J} = \sum_{j \leqslant j', m \geqslant 0} \frac{1}{\sqrt{(1+\delta_{j,j'})}} \beta^{\mu J}_{j,j'} \langle jmj'-m|J0\rangle\, a^+_{jm} a^+_{j'-m}, \tag{7}$$

where the coefficients $\beta^{\mu J}_{j,j'}$ are obtained by identifying the two-particle wave function $D^+_{\mu J}|0\rangle$ with the calculated amplitudes of the excited states of ^{134}Sn. Note that excited $J = 0^+$ states are intepreted as generalized seniority $\nu = 2$ states.

In this framework we calculate the even n-particle model states as seniority $\nu = 0$: $(S^+)^{n/2}|0\rangle$ and as seniority $\nu = 2$: $D^+_{\mu JM}(S^+)^{(n-2)/2}|0\rangle$ states. The odd n-particle model states are calculated as seniority $\nu = 1$ $a^+_{jm}(S^+)^{(n-1)/2}|0\rangle$ states. The squared overlaps between the constructed generalized seniority states and our complete shell model states, labeled SM, are given in the equations below.

For the even Sn isotopes we evaluate the seniority $\nu = 0$ and $\nu = 2$ square overlaps

$$\mathcal{O}^{\nu=0}_{J=0} = |\langle {}^{\rm A}{\rm Sn(SM)}; 0^+|(S^+)^{\frac{n}{2}}|\tilde{0}\rangle|^2 \tag{8}$$

and

$$\mathcal{O}^{\nu=2}_{J_i} = |\langle {}^{\rm A}{\rm Sn(SM)}; J_i\,|D^+_J(S^+)^{\frac{n-2}{2}}|\tilde{0}\rangle|^2, \tag{9}$$

where the $D^+_{\mu J}$ operator corresponding to the lowest state of a given J in ^{134}Sn has been used. For the odd Sn isotopes, the seniority square overlaps are evaluated according to

$$\mathcal{O}^{\nu=1}_{J_i} = |\langle {}^{\rm A}{\rm Sn(SM)}; J_i\,|(S^+)^{\frac{n-1}{2}} a^+_{J_i\,\frac{1}{2}}|\tilde{0}\,\rangle|^2. \tag{10}$$

The vacuum state $|\tilde{0}\rangle$ is the ^{132}Sn core, n is the number of valence neutrons, and the index i labels the different shell model states with the same J. These overlaps are, thus, a measure of the strength of generalized pairing correlations of either the ground state or the various excited states.

D. Even isotopes

A typical feature of the seniority scheme is that the spacing of energy levels is independent of the number of valence particles. Our results for the even-mass tin isotopes (see Table III) show that the spacing between the ground state and the 2^+_1 state is fairly constant throughout the whole sequence of isotopes. This suggests that the 2^+_1 states may be described as one broken pair (seniority $\nu = 2$) upon a ground state condensate of 0^+ pairs where the two-particle pair is defined by the calculated ground state of ^{134}Sn.

The results displayed in Table VI indicate that pairing effects are likely to be important. The 0^+ ground states and the first excited 2^+ states have indeed large seniority $\nu = 0$ and $\nu = 2$ components, respectively. Not unexpectedly, however, these components are gradually decreasing as the number of valence neutrons is increasing. This suggests that the pairing effects become less dominant as one approaches the neutron

TABLE VI. Seniority $\nu=0$ squared overlaps $\mathcal{O}^{\nu=0}_{J=0}$ for the ground states and seniority $\nu=2$ squared overlaps $\mathcal{O}^{\nu=2}_{J_i}$ for the lowest lying eigenstates of the even Sn isotopes.

J^π_i	^{136}Sn	^{138}Sn	^{140}Sn	^{142}Sn
0^+_1	0.967	0.929	0.879	0.797
2^+_1	0.889	0.824	0.743	0.617
4^+_1	0.586	0.728	0.251	0.113
4^+_2	0.314	0.000	0.174	0.231
6^+_1	0.896	0.702	0.657	0.002
6^+_2	0.000	0.000	0.014	0.434
8^+_1	0.002	0.678	0.573	0.355
8^+_2	0.843	0.001	0.023	0.014

drip line. A slight exception is seen for the lowest 4^+ states, for which the pairing strength is strongly fragmented in ^{136}Sn, then concentrated again in ^{138}Sn before being further fragmented in ^{140}Sn and ^{142}Sn.

Our calculations also show that (not listed in the above table), in all even isotopes considered, one of the low-lying 0^+ excited states contains a relatively large seniority $\nu = 2$ component.

Note that in evaluating the overlaps of Eqs. (8) and (9) for Table VI we used S^+ and D^+ operators determined from the two-particle wave functions of ^{134}Sn and kept constant throughout the shell. This is consistent with both our many-body shell model approach and the generalized seniority approach of Talmi. Thus, we have refrained from adjusting the coefficients of Eqs. (8) and (9) as valence pairs are added, despite the fact that this could have given larger overlaps beyond ^{136}Sn.

It is also interesting to point out the behavior of the two 8^+ states listed in Table III. The first 8^+ state in ^{134}Sn is mainly $0h_{9/2}1f_{7/2}$ while the second 8^+ state in ^{134}Sn is almost purely $(0h_{9/2})^2$ and comes at a much higher energy. The lowest 8^+ changes character in ^{136}Sn to a state dominated by the $(1f_{7/2})^4$ configuration, which in a seniority language corresponds to a seniority $\nu = 4$ state. It is first in ^{138}Sn that seniority $\nu = 2$ has a large overlap with the lowest shell model state, with the configuration $(1f_{7/2})^3 0h_{9/2}$ as the dominating one.

E. Odd isotopes

For the odd-mass Sn isotopes the seniority $\nu = 1$ square overlaps of Eq. (10) are displayed in Table VII. These quantities allow us to see how the strengths of the various single-quasiparticle levels of ^{133}Sn evolve as valence neutrons are added. We observe that the single-particle strength is largely preserved for the low-lying $9/2^-$, $7/2^-$, and $3/2^-$ states, although being slowly attenuated with an increasing number of valence nucleons. For higher lying states such as the $5/2^-$ states, the strength is more strongly fragmented due to mixing with neighboring states. Comparing Table VII with Fig. 2 we furthermore see that the higher single-quasiparticle levels are shifted downward as neutron pairs are being added in the $f_{7/2}$ level, signaling again the importance of pair correlations in these nuclei. The $3/2^-$ quasiparticle state, which is at 0.64 MeV in ^{135}Sn and at 0.37 MeV in ^{137}Sn, becomes nearly degenerate with the $7/2^-$ ground state in ^{139}Sn and takes over as ground state in ^{141}Sn. For the $9/2^-$ states, we notice that for ^{135}Sn, it is the second excited state that has the largest seniority $\nu = 1$ overlap. For $1/2^-$ there is a lowest state with a large one-quasiparticle overlap except for ^{137}Sn.

TABLE VII. Seniority $\nu = 1$ squared overlaps $\mathcal{O}^{\nu=1}_{J_i}$ for the lowest lying eigenstates of the odd Sn isotopes.

J^π_i	^{135}Sn	^{137}Sn	^{139}Sn	^{141}Sn
$7/2^-_1$	0.966	0.896	0.813	0.729
$3/2^-_1$	0.005	0.773	0.709	0.689
$3/2^-_2$	0.936	0.088	0.120	0.066
$9/2^-_1$	0.003	0.019	0.580	0.552
$9/2^-_2$	0.176	0.608	0.007	0.002
$9/2^-_3$	0.560	0.000	0.004	0.040
$1/2^-_1$	0.631	0.277	0.368	0.660
$1/2^-_2$	0.223	0.341	0.318	0.018
$1/2^-_3$	0.133	0.138	0.083	0.030
$5/2^-_1$	0.006	0.002	0.008	0.168
$5/2^-_2$	0.272	0.030	0.369	0.357
$5/2^-_3$	0.041	0.308	0.012	0.021
$5/2^-_4$	0.172	0.004	0.005	0.003

The large one-quasiparticle overlaps are also reflected in the fact that the energies of the corresponding states come down in energy as A increases, a feature displayed in Fig. 2 with boldfaced numbers for the states with a large one-quasiparticle content.

IV. CONCLUSIONS

We performed extensive shell model studies of the heavy tin isotopes with up to ten valence neutrons outside the closed ^{132}Sn core. A realistic microscopic effective interaction was derived from a modern meson exchange NN potential using many-body perturbation theory. A generalized seniority analysis was applied to get insights on the pairing structure of the shell model states. The results of our calculations are in good agreement with the few available experimental data. The other results can serve as a guideline for future experiments. Furthermore, a generalized seniority analysis shows that pairing correlations are strong even for systems with ten valence particles, although the strength of the pairing correlations gets reduced as we increase the number of valence neutrons.

[1] P. Bhattacharyya *et al.*, Phys. Rev. Lett. **87**, 062502 (2001).
[2] D. C. Radford *et al.*, Phys. Rev. Lett. **88**, 222501 (2002).
[3] HRIBF newsletter, July 2003, http://www.phy.ornl.gov/hribf/usersgroup/news/jul-03/jul-03.html#B.
[4] I. Dillmann *et al.*, Phys. Rev. Lett. **91**, 162503 (2003).
[5] G. Jakob *et al.*, Phys. Rev. C **65**, 024316 (2002).
[6] J. Terasaki, J. Engel, W. Nazarewicz, and M. Stoitsov, Phys. Rev. C **66**, 054313 (2002).
[7] N. J. Stone *et al.*, Phys. Rev. Lett. **94**, 192501 (2005).
[8] J. Shergur *et al.*, Phys. Rev. C **65**, 034313 (2002).
[9] J. Shergur *et al.*, Phys. Rev. C **72**, 024305 (2005).
[10] J. Shergur *et al.*, Phys. Rev. C **71**, 064321 (2005).
[11] Proposal CERN-INTC-2003-04.
[12] P. Hoff *et al.*, Phys. Rev. Lett. **77**, 1020 (1996).
[13] L. Coraggio, A. Covello, A. Gargano, and N. Itaco, Phys. Rev. C **65**, 051306(R) (2002).
[14] F. Hofmann and H. Lenske, Phys. Rev. C **57**, 2281 (1998).

[15] J. Dobaczewski, W. Nazarewicz, T. R. Werner, J. F. Berger, C. R. Chinn, and J. Decharge, Phys. Rev. C **53**, 2809 (1996).
[16] M. Hjorth-Jensen, T. T. S. Kuo, and E. Osnes, Phys. Rep. **261**, 125 (1995).
[17] I. Talmi, *Contemporary Concepts in Physics* (Harwood Academic Publishers, Chur, Switzerland, 1993), Vol. 7.
[18] R. Machleidt, F. Sammarruca, and Y. Song, Phys. Rev. C **53**, R1483 (1996).
[19] R. Machleidt, Adv. Nucl. Phys. **19**, 189 (1989).
[20] B. A. Brown, N. J. Stone, J. R. Stone, I. S. Towner, and M. Hjorth-Jensen, Phys. Rev. C **71**, 044317 (2005).
[21] G. N. White *et al*., Nucl. Phys. **A644**, 277 (1998).
[22] A. Holt, T. Engeland, E. Osnes, M. Hjorth-Jensen, and J. Suhonen, Nucl. Phys. **A618**, 107 (1997).
[23] R. R. Whitehead, A. Watt, B. J. Cole, and I. Morrison, Adv. Nucl. Phys. **9**, 123 (1977).
[24] T. Engeland, the Oslo shell model code, 1991-2006, unpublished.
[25] K. A. Mezilev, Yu. N. Novikov, A. V. Popov, B. Fogelberg, and L. Spanier, Phys. Scripta T **56**, 272 (1995).
[26] W. Urban *et al*., Eur. Phys. J. A **5**, 239 (1999).
[27] M. Hjorth-Jensen, H. Müther, E. Osnes, and A. Polls, J. Phys. G **22**, 321 (1996).
[28] A. P. Zuker, Phys. Rev. Lett. **90**, 042502 (2003).
[29] A. Korgul *et al*., Eur. Phys. J. A **7**, 167 (2000).
[30] E. Osnes, Ph.D. thesis, University of Oslo, 1966, unpublished.
[31] T. Engeland and E. Osnes, Phys. Lett. **20**, 424 (1966).
[32] D. J. Dean and M. Hjorth-Jensen, Rev. Mod. Phys. **75**, 607 (2003).
[33] A. Bohr and B. R. Mottelson, *Nuclear Structure* (World Scientific, Singapore, 1998), Vol. 1.
[34] C. T. Zhang *et al*., Z. Phys. A **358**, 9 (1997).
[35] G. Bonsignori, M. Savoia, K. Allaart, A. van Egmond, and G. Te Velde, Nucl. Phys. **A432**, 389 (1985).
[36] K. Allaart, E. Boeker, G. Bonsignori, M. Savoia, and Y. K. Gambhir, Phys. Rep. **169**, 209 (1988).